

State-dependent fractional plasticity model for the true triaxial behaviour of granular soil

Y. SUN¹⁾, W. SUMELKA²⁾

¹⁾*Key Laboratory of Ministry of Education for Geomechanics and Embankment Engineering, Jiangsu Research Center for Geotechnical Engineering Technology, Hohai University, Nanjing 210098, China
e-mail: sunny@hhu.edu.cn*

²⁾*Institute of Structural Engineering, Poznan University of Technology, Piotrowo 5, 60-965 Poznań, Poland
e-mail: wojciech.sumelka@put.poznan.pl*

THE FRACTIONAL PLASTICITY WAS PROPOSED TO MODEL THE STRESS-STRAIN BEHAVIOUR of granular soils, but only within the scope of classical triaxial loading condition. In this study an attempt is made to develop a 3D fractional plasticity model for granular soils subjected to true triaxial loads by using characteristic stress, where all the fractional-order and integer-order derivatives can be easily obtained. Without using a plastic potential, the non-associated plastic flow rule is achieved by performing fractional derivatives of the yielding function in the characteristic stress space. The obtained plastic flow direction is found to be influenced by the fractional order, characteristic stress parameter and intermediate stress ratio. To further validate the proposed model, a series of true triaxial test results of different granular soils are simulated, from which good agreement between the model predictions and the corresponding test results is found.

Key words: fractional plasticity, characteristic stress, true triaxial test, granular soil.

Copyright © 2019 by IPPT PAN, Warszawa

1. Introduction

GRANULAR SOILS, SUCH AS THE ROCKFILL MATERIALS USED IN HYDRAULIC ENGINEERING and unbound materials in pavement engineering, usually suffer from complex loading conditions where the three principal stresses are distinct from each other. In these engineering practices, the plastic deformation behaviour of granular soil is usually considered as one of the most important mechanical properties that needs to be investigated thoroughly. However, due to the limitations of the laboratory techniques, classical triaxial test [1–4], biaxial test [5–7] and plain strain test [8] were usually used to study the strength and deformation behaviour of granular soil. However, the stress conditions in those tests were

usually axial-symmetric or two-dimensional, which was different from the actual stress state in the field [9]. Constitutive models [4, 10–14] based on the above test results are thus only appropriate to model the stress-strain behaviour of materials subjected to a simple stress path. For example, considering the pressure and density dependence of aggregates deformation, LI and DAFALIAS [15] proposed a generalised state-dependent constitutive model for sand subjected to drained and undrained triaxial loads. By taking into account the effect of particle breakage on the critical state or phase transformation behaviour of aggregates during triaxial tests [16, 17], a variety of elastoplastic constitutive models for granular soils were proposed by RUSSELL and KHALILI [18], and YAO *et al.* [19], etc. It can be found that the testing and constitutive modelling of geomaterials under axisymmetric loading conditions were significantly developed. However, the correct representation of the stress-strain behaviour of granular soils subjected to 3D loading conditions is still a challenge.

To gain insight into the strength and deformation behaviour of granular soils under 3D loading, true triaxial tests [20, 21] and the associated development of 3D constitutive models [9, 22–24] were often suggested. It was observed from the experimental results [25, 26] that the stress-strain behaviour of granular soil was non-associated and dependent on the applied intermediate stress ratio or Lode’s angle (θ). Traditional plasticity models [13, 15, 18] developed for triaxial loading conditions often intrinsically assumed as the Von-Mises criterion in the π -plane, which cannot capture the actual yielding/failure behaviour of granular soils in general stress space. To solve this problem, a straightforward method by formulating the deviator stress as a function ($g(\theta)$) of the Lode’s angle (θ) was widely suggested. Even though the idea was simple, $g(\theta)$ sometimes resulted in a singularity problem during calculation [27, 28] which made the derived model not easy for some practical engineering conditions. To develop a simple and yet efficient approach, LU *et al.* [29] proposed a non-linear unified strength criterion by assuming a frictional failure of the octahedral plane represented by the characteristic stress. The characteristic stress was defined as a power function of the traditional stress [29]. Based on this strength criterion, MA *et al.* [30] proposed a 3D constitutive model for geomaterials. However, like other existing models [15, 31–33], an additional assumption of the plastic potential surface in addition to the yielding surface was necessarily used to simulate the non-associated plastic flow of granular soil, which resulted in relatively more model parameters. To solve this limitation, SUN and SHEN [34], and LU *et al.* [35] developed a non-associated fractional plasticity model for soils by using the concept of fractional plastic flow [36–38], where the non-associated plastic flow behaviour was captured by using the fractional-order derivatives of the yielding function. However, their model did not consider the dependence of strength and deformation on material state and

hence cannot simulate the 3D state-dependent stress-strain behaviour of granular soils.

Therefore, in this study, an attempt is made to extend the author's previous stress-fractional plasticity model [34, 39] for axisymmetric loading to simulate the state-dependent 3D stress-strain behaviour of granular soil by incorporating the concept of characteristic stress. The paper is structured as follows: Section 2 presents the basic stress and strain notation as well as the definitions of the fractional derivatives, characteristic stress and state parameters; Section 3 introduces the constitutive equations used in this study while Section 4 presents the yielding surface as well as the loading and plastic flow directions. The hardening modulus is given in Section 5. Model parameter identification and validations are shown in Section 6. Section 7 concludes the study.

2. Notations and definitions

2.1. Notation

All the materials discussed in this study are assumed to be homogeneous and isotropic. Compression is considered as positive and tension is negative. In general stress or strain space, totally six independent stress components with the corresponding six strain components are usually needed for a complete description of the stress and strain states of a material [40]. However, the general stress or strain state represented by six components can be easily transformed into an equivalent state represented by three principal stresses or strains. Therefore, for the sake of simplicity, constitutive equations are usually formulated in the multiaxial stress space represented by the first (σ'_1), second (σ'_2) and third (σ'_3) effective principal stresses. Accordingly, the increment of the effective stress tensor ($\dot{\sigma}'$) is expressed as:

$$(2.1) \quad \dot{\sigma}' = [\dot{\sigma}'_1, \dot{\sigma}'_2, \dot{\sigma}'_3]^T,$$

while in this study, the increment of the total strain is attributed to the increments of the elastic and plastic strains. Therefore, the total strain tensor ($\dot{\epsilon}$) under the small strains assumption can be decomposed into two parts, i.e., elastic ($\dot{\epsilon}^e$) and plastic ($\dot{\epsilon}^p$) strain tensors, as

$$(2.2) \quad \dot{\epsilon} = \dot{\epsilon}^e + \dot{\epsilon}^p,$$

where the incremental elastic tensor $\dot{\epsilon}^e = [\dot{\epsilon}_1^e, \dot{\epsilon}_2^e, \dot{\epsilon}_3^e]^T$ and the incremental plastic strain tensor $\dot{\epsilon}^p = [\dot{\epsilon}_1^p, \dot{\epsilon}_2^p, \dot{\epsilon}_3^p]^T$, the superscripts, e and p , indicate the elastic and plastic components. σ'_1 , σ'_2 and ϵ_3 are the first, second and third principal strains, respectively.

In addition to the principal stresses and strains, the mean effective principal stress (p'), deviator stress (q) and intermediate principal stress ratio (b) are also used in the model derivation:

$$(2.3) \quad p' = \frac{1}{3}(\sigma'_1 + \sigma'_2 + \sigma'_3),$$

$$(2.4) \quad q = \frac{1}{\sqrt{2}}[(\sigma'_1 - \sigma'_2)^2 + (\sigma'_2 - \sigma'_3)^2 + (\sigma'_1 - \sigma'_3)^2]^{1/2},$$

$$(2.5) \quad b = \frac{\sigma'_2 - \sigma'_3}{\sigma'_1 - \sigma'_3}.$$

2.2. Definitions

In this section, three important definitions, i.e., the left-sided Caputo's fractional derivative [41], characteristic stress [29] and state parameter [42], are introduced.

(a) Caputo's fractional derivative

Historically, fractional derivative has been applied to many theoretical analyses of different physical phenomena, as reviewed by ZHANG *et al.* [43]. It was found that different definitions of the fractional derivative were usually suggested when dealing with different physical problems. However, for the sake of simplicity, the well-known Caputo's fractional derivative where the derivation of a constant equals to zero is used in this study. To model the positive and negative dilatancy behaviour of granular soil, the following Caputo's fractional derivative with the fractional order, α , ranging between $n-1$ and n ($n > 0$, is an integer) is suggested:

$$(2.6a) \quad {}_{0^+}D_{\sigma'}^{\alpha} f(\sigma') = \frac{1}{\Gamma(n-\alpha)} \int_{0^+}^{\sigma'} \frac{f^{(n)}(\chi) d\chi}{(\sigma' - \chi)^{\alpha+1-n}}, \quad \sigma' > 0,$$

$$(2.6b) \quad {}_{\sigma'}D_{0^-}^{\alpha} f(\sigma') = \frac{(-1)^n}{\Gamma(n-\alpha)} \int_{\sigma'}^{0^-} \frac{f^{(n)}(\chi) d\chi}{(\chi - \sigma')^{\alpha+1-n}}, \quad \sigma' < 0,$$

where D ($= \partial^{\alpha}/\partial\sigma'^{\alpha}$) denotes derivation while σ' is the effective loading stress in this study; f is the yielding function in this study and Γ is the the gamma function. A clear integral definition of the Caputo's fractional derivative is observed in Eq. (2.6) where the stress memory from load onset to current load state can be intrinsically considered.

It should be noted that there are only the limited number of analytical solutions of the fractional derivatives. Most mathematical functions can only be solved by a numerical method, for example, the finite difference method and the

finite element method [44]. Fortunately, the explicit solution of a power function $((x - a)^\varsigma)$ that is often encountered in plastic yielding or potential functions exists. By substituting $(x - a)^\varsigma$ into Eq. (2.6), one has

$$(2.7) \quad {}_a D_x^\alpha (x - a)^\varsigma = \frac{\Gamma(1 + \varsigma)}{\Gamma(1 + \varsigma - \alpha)} (x - a)^{\varsigma - \alpha},$$

where $\varsigma > -1$, is the power index, ensuring the integrability of Eq. (2.7). In this study, $a = 0$. Hence, the modified Cam-clay yielding surface with power-law functions is used in this study to facilitate further model implementation.

(b) Characteristic stress

To develop an unified strength criterion for geomaterials in a simple way, LU *et al.* [29] proposed a concept of characteristic stress, which is denoted as $\bar{\sigma}'_i = \bar{\sigma}'_i(\sigma'_i)$. $\bar{\sigma}'_i$ is obtained by combining the classical stress notation, σ'_i , with a characteristic parameter, β , as

$$(2.8) \quad \bar{\sigma}'_i = p_a \left(\frac{\sigma'_i}{p_a} \right)^\beta,$$

where $i = 1, 2, 3$; $p_a = 100$ kPa, is the atmospheric pressure for the purpose of parameter nondimensionalization; β ranges from 0 to 1 and is used to reflect the effect of intermediate principal stress on the yielding behaviour of granular soil. As proved by LU *et al.* [29] and MA *et al.* [30], the value of β is constant and independent of the density and pressure of a certain material. The relevant characteristic effective mean principal and deviator stresses can be further defined respectively as:

$$(2.9) \quad \bar{p}' = \frac{1}{3}(\bar{\sigma}'_1 + \bar{\sigma}'_2 + \bar{\sigma}'_3),$$

$$(2.10) \quad \bar{q}' = \frac{1}{\sqrt{2}}[(\bar{\sigma}'_1 - \bar{\sigma}'_2)^2 + (\bar{\sigma}'_2 - \bar{\sigma}'_3)^2 + (\bar{\sigma}'_1 - \bar{\sigma}'_3)^2]^{1/2}.$$

(c) State parameter

It has been widely recognised that the stress-strain and dilatancy behaviour of granular soil is significantly dependent on its density and pressure [1, 12, 42]. To model such dependence of material state (density and pressure), various state parameters have been suggested, for example, the state ratio of the difference between the threshold and current void ratios to the difference between the threshold and critical void ratios proposed by ISHIHARA [45], the ratio of the current to critical void ratios suggested by WAN and GUO [46], and the ratio of the current to critical mean effective stresses suggested by WANG *et al.* [47]. However, the most widely used state parameter (ψ) was proposed by BEEN and

JEFFERIES [42] as

$$(2.11) \quad \psi = e - e_c,$$

where e is the current void ratio; e_c is the critical state void ratio, which can be defined as [48]

$$(2.12) \quad e_c = e_\Gamma - \lambda \left(\frac{p'}{p_a} \right)^\xi,$$

where e_Γ , λ , and ξ are the critical state parameters in the $e - p'$ plane. ψ is positive when the material is consolidated at the ‘wet’ side of the critical state line, and is negative for materials at the ‘dry’ side. Due to its simplicity, the state parameter, ψ , is used in this study for further constitutive modelling.

3. Constitutive equations

As the total strain can be decomposed into the elastic and plastic components, the following elastoplastic constitutive relationship can be given [49]:

$$(3.1) \quad \dot{\epsilon}_i = (C_{ij}^e + C_{ij}^p) \dot{\sigma}'_j,$$

where the elastic compliance matrix can be expressed as:

$$(3.2) \quad C_{ij}^e = \frac{1}{2G(1+\nu)} \quad \text{for } i = j,$$

$$(3.3) \quad C_{ij}^e = \frac{-\nu}{2G(1+\nu)} \quad \text{for } i \neq j,$$

where ν is the Poisson’s ratio; the shear modulus G can be expressed as [15]:

$$(3.4) \quad G = G_0 \frac{(2.97 - e)^2}{1 + e} p_a \sqrt{\frac{p'}{p_a}},$$

in which G_0 is the dimensionless elastic parameter of the material. The value of 2.97 in Eq. (3.4) was proposed by HARDIN and RICHART [50] based on a comprehensive laboratory evaluation of a variety of granular soils. The plastic compliance matrix is formulated as

$$(3.5) \quad C_{ij}^p = \frac{1}{H} m_i n_j,$$

where H is the hardening modulus and is defined later; $i, j = 1, 2$ and 3 ; m_i and n_j are components of the plastic flow and loading tensors, respectively, related

to the effective principal stress σ'_i . Therefore, the loading and plastic flow components can be further obtained, respectively, as:

$$(3.6) \quad n_i = \frac{L_i}{L},$$

$$(3.7) \quad m_j = \frac{F_j}{F},$$

where the loading related component L_i can be obtained by using the chain rule as

$$(3.8) \quad L_i = \frac{\partial f}{\partial \bar{p}'} \frac{\partial \bar{p}'}{\partial \sigma'_i} + \frac{\partial f}{\partial \bar{q}} \frac{\partial \bar{q}}{\partial \sigma'_i},$$

while L is defined as

$$(3.9) \quad L = \sqrt{L_1^2 + L_2^2 + L_3^2}.$$

The plastic flow related component F_j is obtained by performing the fractional order derivative of the yielding surface as [39]. However, it is noted that the chain rule may not be able to be used in conducting fractional order derivatives [51] of a certain function. Therefore, to avoid confusion, the plastic flow tensor is obtained by directly conducting derivative with respect to the principal characteristic stress:

$$(3.10) \quad F_j = \frac{\partial^\alpha f}{\partial \sigma_j'^\alpha},$$

$$(3.11) \quad F = \sqrt{F_1^2 + F_2^2 + F_3^2}.$$

As detailly elucidated in [39] and [34], different plastic flow directions can be obtained by changing the value of the fractional order. The larger the value of α is, the more non-coaxial the directions of stress and strain increments are.

4. Loading and plastic flow tensors

4.1. Yielding surface

Following LU *et al.* [29] and MA *et al.* [30], the modified Cam-clay yielding function is expressed in the characteristic stress space as:

$$(4.1) \quad f = \bar{M}^2 \bar{p}'^2 + \bar{q}^2 - \bar{M}^2 \bar{p}'_0 \bar{p}' = 0,$$

where \bar{p}'_0 represents the intercept of the yielding surface with the \bar{p}' -axis and it controls the size of the yielding surface; \bar{M} is the critical state stress ratio in the characteristic stress space and can be determined by:

$$(4.2) \quad \bar{M} = \frac{\bar{q}_c}{\bar{p}'_c} = 3 \frac{(1 + \sin \phi_c)^\beta - (1 - \sin \phi_c)^\beta}{(1 + \sin \phi_c)^\beta + 2(1 - \sin \phi_c)^\beta},$$

where the subscript c indicates critical state; ϕ_c is the critical state friction angle at $b = 0$. As shown in Fig. 1, the 3D yielding surface generated by using the characteristic stress approach is orthogonal to the p' -axis. Unlike classical

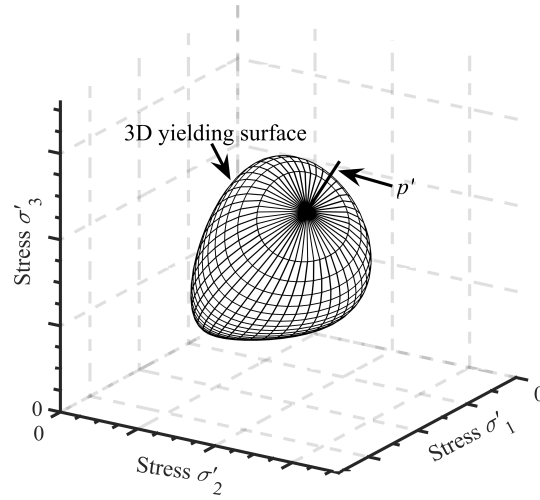


FIG. 1. 3D yielding surface in the effective principal stress space.

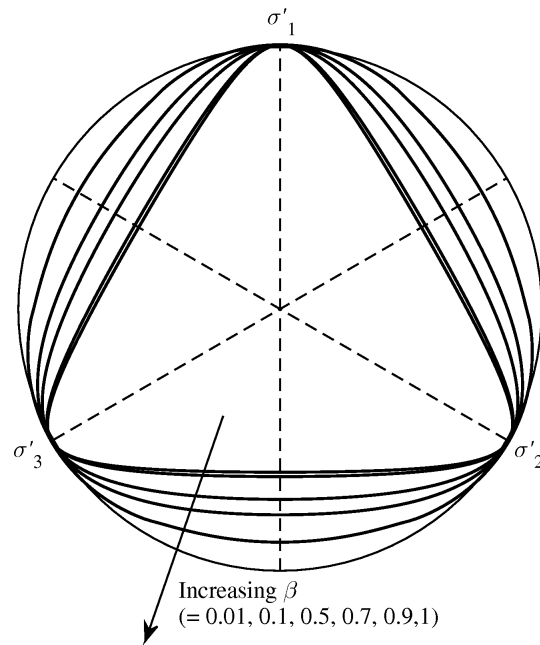


FIG. 2. Yielding curve in the π plane.

yielding surfaces, a triaxial axisymmetric surface in the σ'_i space can be achieved even without the use of a $g(\theta)$ function, as shown in Fig. 2. With the increase of β , the yielding/failure curve in the π plane becomes less triangle and approach the circle resented by the Drucker–Prager criterion [52]. Therefore, the 3D yielding/failure properties can be characterised by using Eqs. (2.8)–(2.10) and (4.1). It is noted that when $\beta = 1$, \bar{M} equals M ($= 6 \sin \phi_c / (3 - \sin \phi_c)$), the proposed model reduces to the classical Drucker–Prager one.

4.2. Loading tensor

The loading direction should be perpendicular to the yielding surface. Therefore, it can be obtained by substituting Eq. (4.1) into Eqs. (3.6), (3.8) and (3.9)

$$(4.3) \quad n_i = \frac{1}{L} \left[\frac{1}{3} (M^2 \bar{p}' - \bar{q}^2 / \bar{p}') + 3(\bar{\sigma}'_i - \bar{p}') \right],$$

where the loading amplitude L is formulated as:

$$(4.4) \quad L = \sqrt{\sum_{i=1}^3 \left[\frac{1}{3} (M^2 \bar{p}' - \bar{q}^2 / \bar{p}') + 3(\bar{\sigma}'_i - \bar{p}') \right]^2}.$$

4.3. Plastic flow tensor

The plastic flow direction should be non-perpendicular to the yielding surface, which can be obtained by performing fractional derivative on the yielding surface [36]. Accordingly, substituting Eq. (4.1) into Eqs. (3.7), (3.10) and (3.11)

$$(4.5) \quad m_j = \frac{1}{F} \left[\frac{\bar{\sigma}_j^{1-\alpha}}{\Gamma(2-\alpha)} (A \bar{\sigma}_j^- 3\bar{p}' + B/3) \right],$$

where

$$(4.6) \quad A = 2 \left(\frac{\bar{M}}{3} \right)^2 \frac{\alpha - 1}{2 - \alpha} + \frac{4 - \alpha}{2 - \alpha},$$

$$(4.7) \quad B = \bar{M}^2 \bar{p}' - \frac{\bar{q}^2}{\bar{p}'},$$

$$(4.8) \quad F = \sqrt{\sum_{j=1}^3 \left[\frac{\bar{\sigma}_j^{1-\alpha}}{\Gamma(2-\alpha)} (A \bar{\sigma}_j^- 3\bar{p}' + B/3) \right]^2}.$$

Comparing Eq. (4.5) with Eq. (4.3), it can be easily found that $m_j = n_i$ when $\alpha = 1$. A non-associated plastic flow rule can be considered by using

$$(4.9) \quad \alpha = e^{\Delta\psi}$$

where $\Delta > 0$, is a material constant. By correlating α with the state parameter ψ , the state-dependent plastic flow which is commonly observed in granular soils, can be considered. For dense materials with $\psi < 0$, they experience strain softening and volume dilation which can be modelled by using $0 < \alpha < 1$. During shearing, ψ and the associated α increase; materials gradually approach the critical state where $\psi = 0$ and $\alpha = 1$. For loose materials with $\psi > 0$ they experience strain hardening and volume contraction which is characterised by $\alpha > 1$.

The stress-dilatancy ratio (d) can be further obtained as:

$$(4.10) \quad d = \frac{m_v}{m_s} = \frac{\bar{M}^2 - (1 - \alpha/2)[\bar{\eta}^2 + \bar{M}^2]}{\bar{\eta}^{2-\alpha}},$$

where m_v and m_s are the plastic flow components with regard to \bar{p}' and \bar{q} , respectively; and the characteristic stress ratio is $\bar{\eta} = \bar{q}/\bar{p}'$. Figure 3 represents the relationship between the dilatancy ratio d and stress ratio η ($= q/p'$) under different intermediate stress ratios. As can be observed, by using a proper value of α or β , stress-dilatancy behaviours under different b -values are simulated. For example, a downward shifting of the stress-dilatancy curve with the increase

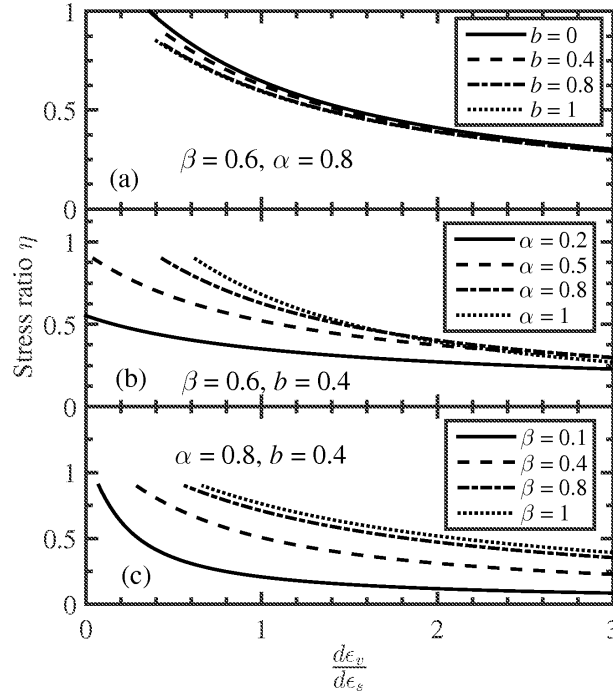


FIG. 3. Characteristic fractional stress-dilatancy relationship.

of b can be found in Fig. 3(a). With the decrease of η , the stress-dilatancy curves in Fig. 3(a) approach more with each other, indicating no plastic shear strain occurs at isotropic stress states. Similar observations were also reported by MA *et al.* [30]. Figure 3(b) shows the effect of α on the stress-dilatancy behaviour, where an upward shifting of the stress-dilatancy curve with an increase of α is observed. More details of the effect of α can be found in [14]. Figure 3(c) shows the effect of β on the stress-dilatancy curve, from which an upward shifting of the stress-dilatancy curve with the increasing β is observed.

5. Hardening modulus

The hardening modulus used for modelling granular soils under triaxial loading conditions ($b = 0$) is modified here to account for the 3D strength and deformation characteristics. According to LI and DAFALIAS [15], the hardening modulus H should satisfy the following conditions: (i) $H = +\infty$ at $\bar{\eta} = 0$, (ii) $H = 0$ at the critical state stress points and (iii) $H = 0$ at the drained peak stress points. Therefore, the hardening modulus H can be expressed as:

$$(5.1) \quad H = hG \left(\frac{\bar{M}_p}{\bar{\eta}} - 1 \right) \exp(k\psi),$$

where the peak stress ratio \bar{M}_p is defined as

$$(5.2) \quad \bar{M}_p = \bar{M} \exp(-k\psi),$$

where k is a material constant, describing the influence of ψ on \bar{M}_p and H . $\bar{M}_p = \bar{M}$ when $\psi = 0$. The hardening parameter h can be expressed as:

$$(5.3) \quad h = (h_1 - h_2 e)$$

where h_1 and h_2 are material constants. The expression of h in Eq. (5.3) is different from that in [14]. Following the suggestions by LI and DAFALIAS [15], the current void ratio (e) instead of the initial void ratio (e_0) is used. It should be noted that the different definitions of h using e or e_0 could result in the different performances in model simulation, as shown in Figs. 4–5. Figures 4(a) and 5(a) show the improved model predictions of the constitutive behaviour of Toyoura sand [53] using e while Figs. 4(b) and 5(b) represent the original model predictions using e . It can be found that the use of e_0 instead of e would make the model underestimate the deviator stress. With the increase of e_0 , the extent of such underestimation increases. For example, the original model prediction with $e_0 = 0.996$ reported a significant lower deviator stress than the corresponding experimental result. However, it should be noted that: such prediction

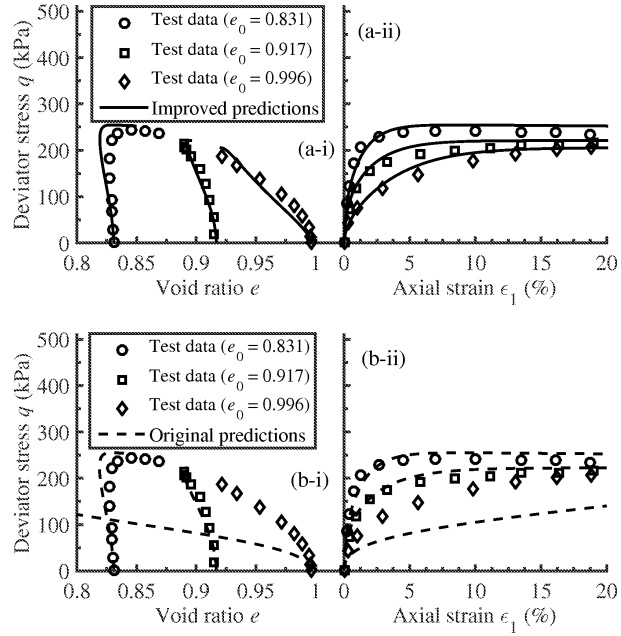


FIG. 4. Stress-strain behaviour of Toyoura sand predicted by using (a) e and (b) e_0 ($\sigma'_3 = 100$ kPa).

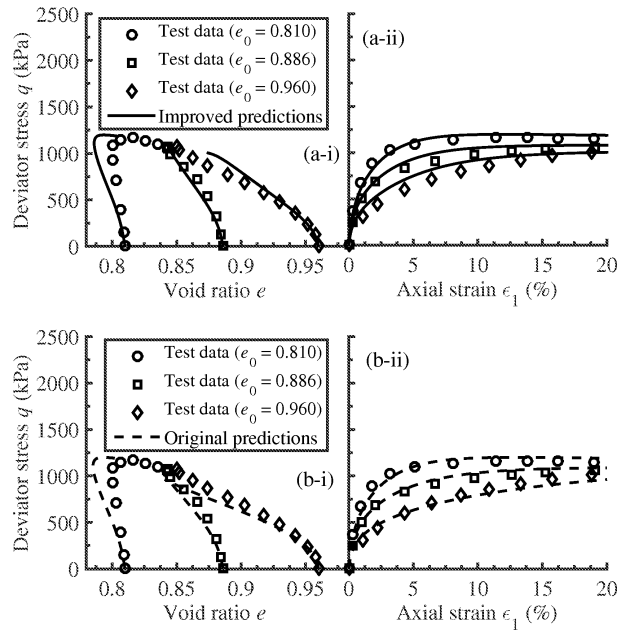


FIG. 5. Stress-strain behaviour of Toyoura sand predicted by using (a) e and (b) e_0 ($\sigma'_3 = 500$ kPa).

difference can be remedied by tuning the hardening parameters, h_1 and h_2 , as shown in [15]. Nevertheless, this kind of modification shown in Eq. (5.3) attempts to make the model more reasonable for practical engineering. This is owing to the consideration that e_0 should be unknown for samples that have already been sheared where only e can be evaluated. As can be expected from Eqs. (5.1)–(5.3), the value of H depends on several factors, such as the pressure and density (e, e_0, \bar{p}', ψ), shear modulus (G), and the difference between the characteristic stress ratios ($\bar{M}_p - \bar{\eta}$). H can be positive with $\bar{M}_p > \bar{\eta}$ where the states of strain hardening and volume contraction can be modelled. H can be also positive with $\bar{M}_p < \bar{\eta}$ where the state of strain softening and volume dilation can be captured.

6. Model validation

6.1. Parameter identification

This model has eleven parameters to simulate the 3D stress-strain behaviour of granular soil. There are four critical state parameters ($\phi_c, \lambda, e_\Gamma, \xi$), three hardening parameters (k, h_1, h_2), two elastic constants (G_0, ν), one characteristic stress parameter (β) and one fractional parameter (Δ). Most parameters can be determined from compression test results at $b = 0$. Detailed discussions on how to determine these parameters are presented as follows.

The four critical state parameters ($\phi_c, \lambda, e_\Gamma, \xi$) determine the critical state behaviour of granular soil. The critical state friction angle, ϕ_c , can be determined through triaxial compression test. It is related to the gradient (M) of the critical state line in the $p' - q$ plane as

$$(6.1) \quad \phi_c = \arcsin \left(\frac{3M}{6 + M} \right),$$

The other three parameters (λ, e_Γ, ξ) can be determined by fitting the critical state data points in the $e - p'$ planes, as shown in [48].

The parameter k defines the peak stress state of the material. It can be determined by the peak stress points of materials subjected to triaxial compression where $H = 0$, i.e.

$$(6.2) \quad k = \frac{1}{2\psi_p} \ln \frac{\bar{M}}{\eta_p},$$

where ψ_p and η_p are two values of ψ and η at the peak stress state. The hardening parameters, h_1 and h_2 , determine the hardening and softening behaviour of the material. h_1 and h_2 can be obtained by fitting the $\varepsilon_1 - q$ relationship at different material states, as illustrated in [34].

The characteristic parameter, β , controls the failure shape of the yielding function in the π plane. According to LU *et al* [29] and MA *et al.* [30], it can be determined by the critical state friction angles (ϕ_c, ϕ_e) at triaxial compression and extension states, i.e.

$$(6.3) \quad \frac{(1 + \sin \phi_c)^\beta - (1 - \sin \phi_c)^\beta}{(1 + \sin \phi_c)^\beta + 2(1 - \sin \phi_c)^\beta} = \frac{(1 + \sin \phi_e)^\beta - (1 - \sin \phi_e)^\beta}{2(1 + \sin \phi_e)^\beta + (1 - \sin \phi_e)^\beta}.$$

However, it could be also simply determined by fitting the failure data of granular soil in the π plane. According to MA *et al.* [30], the strength curves by using the characteristic stress method almost coincide with each other and resemble the Matsuoka–Nakai criterion [54] when $\beta \leq 0.1$; $\beta = 0.1$, was suggested to model the 3D strength characteristic of granular soils [29, 30] for simplicity. The fractional parameter, Δ , controls the plastic flow of granular soil. It can be obtained by using Eq. (4.10) at the phase transformation state in triaxial tests where $d = 0$. Hence,

$$(6.4) \quad \Delta = \frac{1}{\psi_d} \ln \frac{2}{1 + (\bar{M}/\bar{\eta}_d)^2},$$

where $\bar{\eta}_d$ is the value of $\bar{\eta}$ and $\psi_d = e_d - e_c$ at the phase transformation state, measured from the drained or undrained test.

The elastic constants (G_0, ν) can be obtained from the $\varepsilon_1 - q$ relationship during the initial loading stage. By using Eq. (3.4), G_0 can be determined as:

$$(6.5) \quad G_0 = \frac{(1 + e)G}{(2.97 - e)^2 \sqrt{p' p_a}},$$

$$(6.6) \quad \nu \approx \frac{3\varepsilon_s - 2\varepsilon_v}{6\varepsilon_s + 2\varepsilon_v}.$$

The detailed values of the model parameters for different granular soils are listed in Table 1.

Table 1. Model parameters.

Soil type	G_0	ν	$\phi_c(^{\circ})$	λ	e_r	ξ	β	Δ	k	h_1	h_2
Toyoura sand [53]	125	0.05	31.2	0.019	0.934	0.7	0.1	0.01	1.1	4.5	4.5
Rockfill G1 [9]	90	0.25	46	0.110	0.404	0.1	0.1	0.2	0.1	1.2	0.3
Rockfill G2 [9]	90	0.25	51	0.024	0.314	0.3	0.1	0.5	10	1.0	1.0

6.2. Model prediction

A series of true triaxial tests on the granite rockfill reported by XIAO *et al.* [9] are used in this study to validate the proposed model. The rockfill aggregates

were collected from the construction site of the Shuangjiangkou core-wall rock-fill dam. Two different gradings were used for the test. Grading No. 1 (G1) had a maximum particle size (d_M) of 5 mm and a minimum particle size (d_m) of 2 mm while grading No. 2 (G2) had a d_M of 10 mm and a d_m of 0.075 mm. The initial sample size for G1 was 70 mm \times 70 mm \times 35 mm while the one for G2 was 120 mm \times 120 mm \times 60 mm. The initial void ratios were 0.68 and 0.26 for G1 and G2, respectively. The true triaxial apparatus (TTA) designed and built in Hohai University was used to conduct the test. It was reported that the TTA possessed a stress-controlled flexible boundary in the lateral direction (σ'_3 -axis) and two strain-controlled rigid boundaries in lateral (σ'_2 -axis) and vertical (σ'_1 -axis) directions. Detailed descriptions of the TTA, specimen preparation and test procedures can be found in [55] and thus not repeated here for simplicity.

Figures 6–9 show the model simulations of the 3D stress strain behaviour of the rockfill G1 subjected to different true triaxial test conditions. Five different intermediate principal stress ratios of 0, 0.25, 0.5, 0.75 and 1.0 with four different third effective principal stresses of 100 kPa, 125 kPa, 150 kPa and 200 kPa were used for the true triaxial tests on rockfill G1. It can be observed

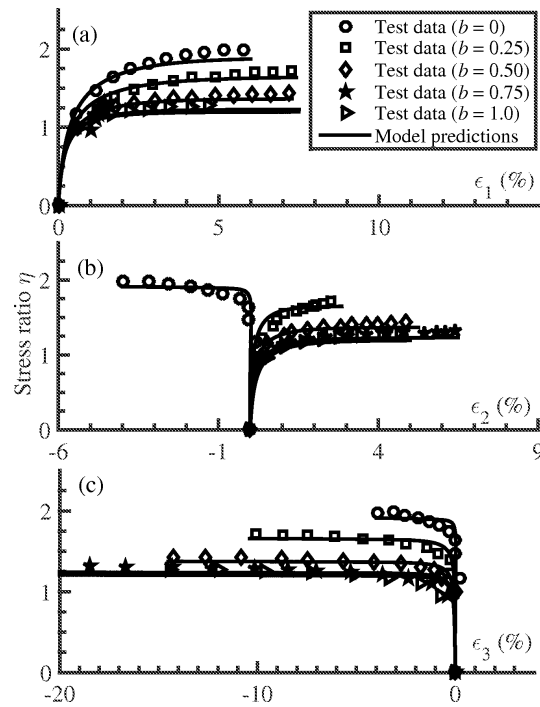


FIG. 6. Model predictions of the 3D stress strain behaviour of rockfill G1 at $\sigma'_3 = 100$ kPa.

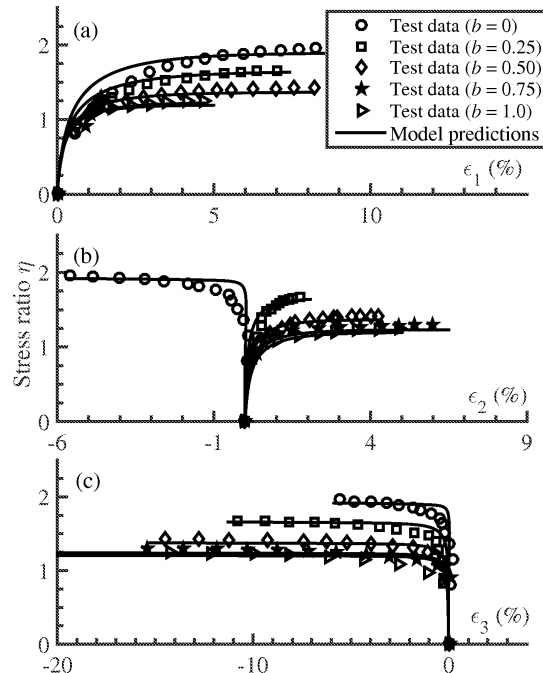


FIG. 7. Model predictions of the 3D stress strain behaviour of rockfill G1 at $\sigma'_3 = 125$ kPa.

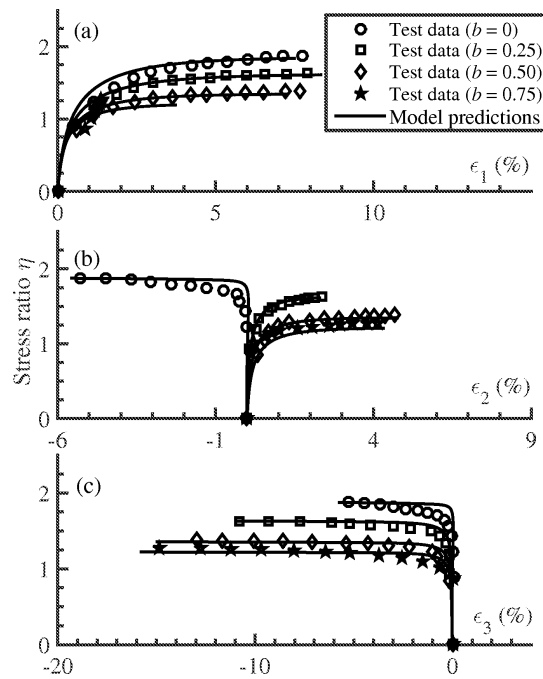


FIG. 8. Model predictions of the 3D stress strain behaviour of rockfill G1 at $\sigma'_3 = 150$ kPa.

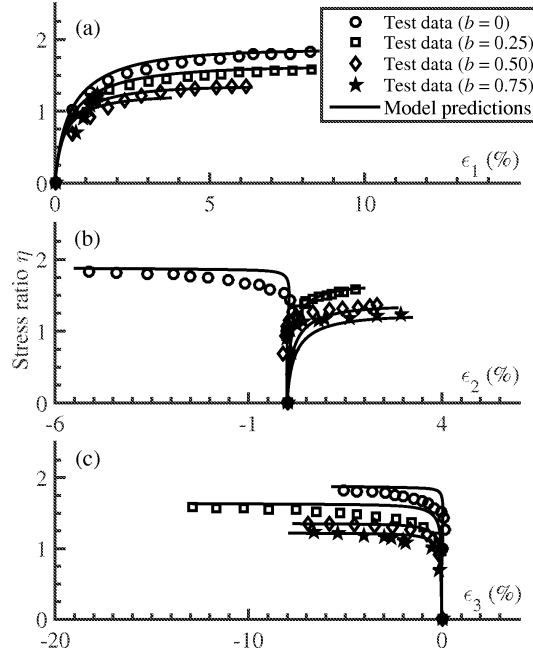


FIG. 9. Model predictions of the 3D stress strain behaviour of rockfill G1 at $\sigma'_3 = 200$ kPa.

that the characteristic stress-based fractional plasticity model can well capture the 3D stress-strain behaviour of the rockfill G1 under different loading conditions. Specifically, the first and third principal strains during the entire shearing process were positive and negative, respectively, irrespective of the intermediate principal stress ratio and the third effective principal stress, which can be accurately predicted by the proposed model. Moreover, the model can also reasonably characterise the negative second principal strain with $b = 0$ and the positive one with b larger than 0.25, which highlights the rationality of the developed state-dependent fractional plastic flow rule. By using the extended 3D hardening modulus shown in Eq. (5.1), the decreasing stress ratio of rockfill G1 with the increase of the intermediate stress ratio and third effective principal stress is also captured by the model.

Figures 10–15 show the model predictions of the 3D stress-strain behaviour of the rockfill G2 subjected to different true triaxial loading conditions. Five different intermediate principal stress ratios of 0, 0.25, 0.5, 0.75 and 1.0 with six different third effective principal stresses of 150 kPa, 200 kPa, 250 kPa, 300 kPa, 350 kPa and 400 kPa were used for the tests on the rockfill G2. Figures 10(a)–15(a) show the model simulations of the test results represented by the first principal strain v.s. stress ratio while Figs. 10(b)–15(b) show the model simulations of the test results represented by the second principal strain v.s.

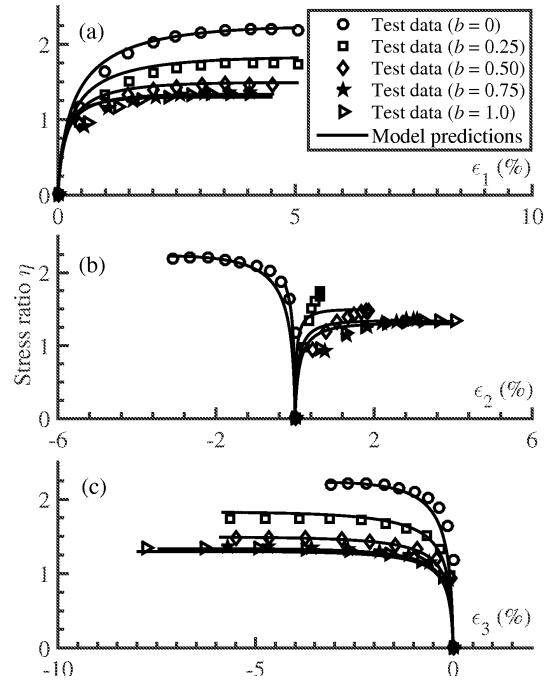


FIG. 10. Model predictions of the 3D stress strain behaviour of rockfill G2 at $\sigma'_3 = 150$ kPa.

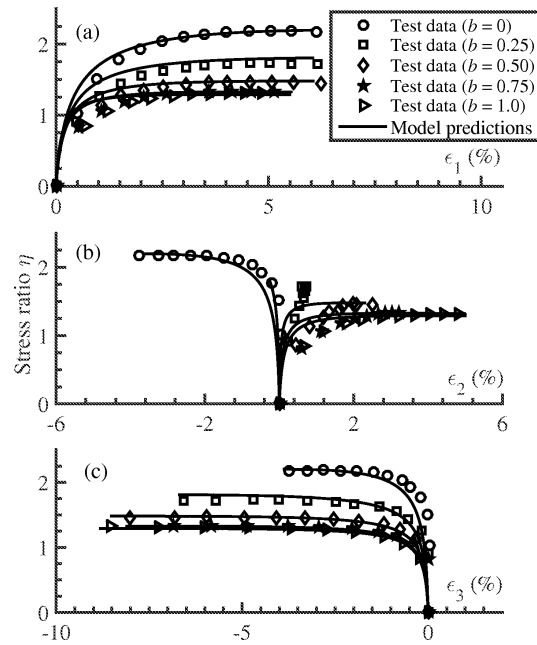


FIG. 11. Model predictions of the 3D stress strain behaviour of rockfill G2 at $\sigma'_3 = 200$ kPa.

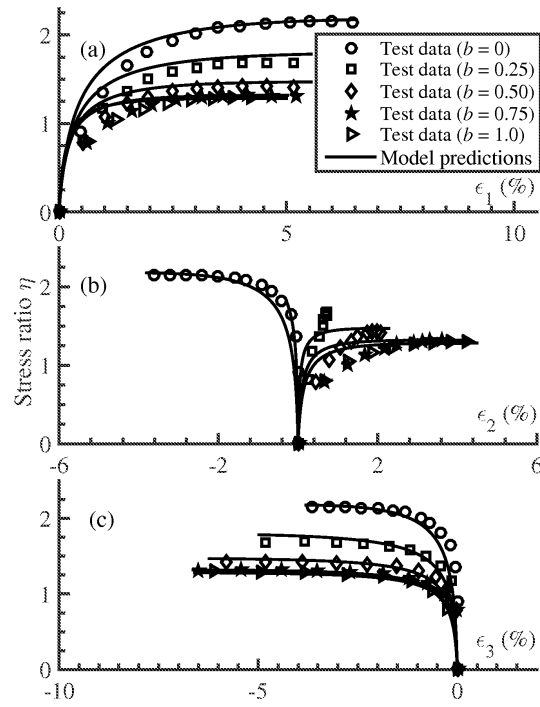


FIG. 12. Model predictions of the 3D stress strain behaviour of rockfill G2 at $\sigma'_3 = 250$ kPa.

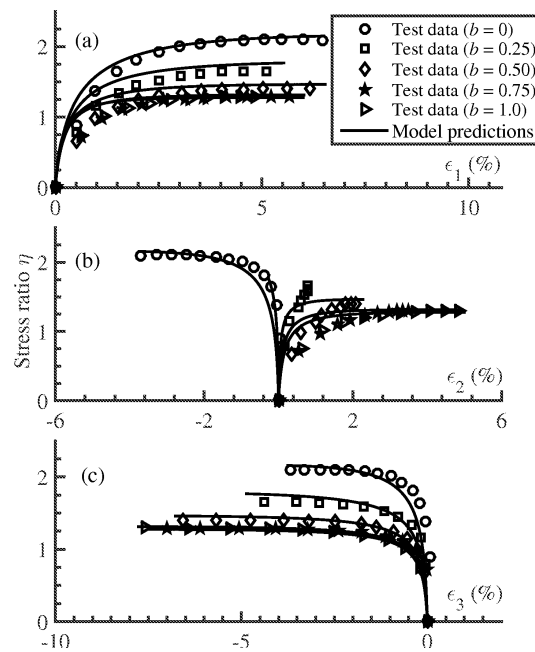


FIG. 13. Model predictions of the 3D stress strain behaviour of rockfill G2 at $\sigma'_3 = 300$ kPa.

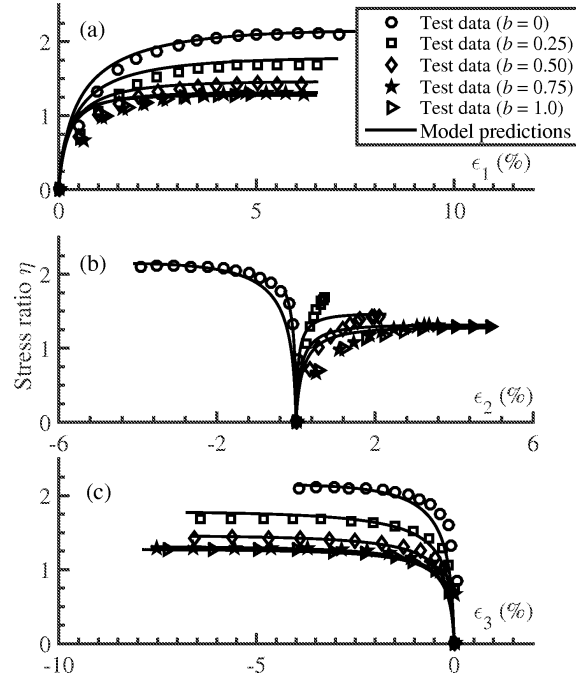


FIG. 14. Model predictions of the 3D stress strain behaviour of rockfill G2 at $\sigma'_3 = 350$ kPa.

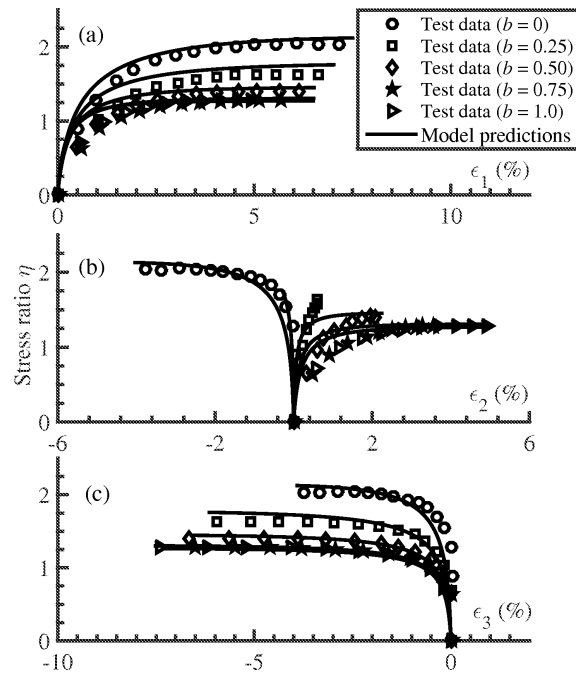


FIG. 15. Model predictions of the 3D stress strain behaviour of rockfill G2 at $\sigma'_3 = 400$ kPa.

stress ratio. The evolutions of the third principal strain v.s. stress ratio are shown in Figs. 10(c)–15(c). As it can be observed, by using the concept of characteristic stress, the developed 3D state-dependent fractional plasticity model can also well simulate the stress-strain behaviour of the rockfill G2 under different initial and loading states in the 3D stress-strain space.

7. Conclusions

The stress-strain behaviour of granular soil depends on the material state and loading condition. However, most constitutive models developed for triaxial loading did not consider the 3D strength characteristic of granular soil and thus cannot capture its 3D stress-strain behaviour. To solve this problem, a state-dependent stress-fractional plasticity model based on the concept of characteristic stress was proposed in this study. There were eleven parameters of the proposed model, which can be all determined from the true triaxial test results. Sensitive analysis of some model parameters and detailed approaches on how to obtain parameter values were presented and discussed. Model validations were then carried out by simulating a series of true triaxial test results of two different rockfills. The main conclusions are summarised as follows:

(1) By simply incorporating the characteristic stress into the modified Cam-clay yielding function, a 3D yielding surface in the effective principal stress space was obtained. It was found that a curved triangular shape of the yielding curve in the π plane was achieved. With the increase of the characteristic parameter, the yielding curve in the π plane resembled more a circle as represented by the Drucker-Prager criterion. Insignificant differences were observed between the yielding curves with the characteristic parameter less than 0.1.

(2) Without using any additional assumption of the plastic potential surface, a generalised non-associated fractional plastic flow rule for granular soils subjected to 3D loading condition was proposed by using the fractional derivative and characteristic stress. Unlike previous models developed under triaxial loads, the derived plastic flow rule was significantly influenced by the intermediate principal stress ratio. With the increase of the intermediate principal stress ratio, the stress-dilatancy curve shifted downwards. For soils subjected to fixed intermediate principal stress ratio, the stress-dilatancy curve shifted upwards with the increasing fractional order and characteristic parameter.

(3) The original hardening modulus for triaxial loads was extended for 3D stress conditions by incorporating the characteristic stress. The derived 3D hardening modulus considered the influences of material density and stress condition. It can reproduce the hardening and softening phenomenon of granular soil. The use of the current void ratio instead of the initial void ratio would improve model

performance. A lower deviator stress would be predicted if the initial void ratio was used.

(4) The established 3D fractional plasticity model was able to capture the stress-strain behaviour of granular soils subjected to different true triaxial test conditions. The predicted stresses and principal strains matched well with the corresponding test results.

Acknowledgements

In memory of the mentor, Prof. Wen Chen, who inspired the first author for a lifelong time. The support from the Natural Science Foundation of China (Grant Nos. 41630638, 51679068), the National Key Basic Research Program of China (“973” Program) (Grant No. 2015CB057901), the Fundamental Research Funds for the Central Universities (Grant No. 2017B05214) and the China Post-doctoral Science Foundation (Grant No. 2017M621607) are appreciated. The second author also acknowledges the support of the National Science Centre, Poland, under Grant No. 2017/27/B/ST8/00351.

References

1. X. KONG, J. LIU, D. ZOU, H. LIU, *Stress-dilatancy relationship of Zipingpu gravel under cyclic loading in triaxial stress states*, International Journal of Geomechanics, **16**, 04016001, 2016.
2. A.S. SUIKER, E.T. SELIG, R. FRENKEL, *Static and cyclic triaxial testing of ballast and subballast*, Journal of Geotechnical and Geoenvironmental Engineering, **131**, 771–782, 2005.
3. Y. XIAO, H. LIU, Y. CHEN, J. JIANG, *Strength and deformation of rockfill material based on large-scale triaxial compression tests. I: influences of density and pressure*, Journal of Geotechnical and Geoenvironmental Engineering, **140**, 04014070, 2014.
4. Z.Y. YIN, C.S. CHANG, P.Y. HICHER, M. KARSTUNEN, *Micromechanical analysis of kinematic hardening in natural clay*, International Journal of Plasticity, **25**, 1413–1435, 2009.
5. C. NOUGUIER-LEHON, *Effect of the grain elongation on the behaviour of granular materials in biaxial compression*, Comptes Rendus Mécanique, **338**, 587–595, 2010.
6. M. MUKHERJEE, A. GUPTA, A. PRASHANT, *Drained instability analysis of sand under biaxial loading using a 3D material model*, Computers and Geotechnics, **79**, 130–145, 2016.
7. G. MA, W. ZHOU, X.-L. CHANG, *Modeling the particle breakage of rockfill materials with the cohesive crack model*, Computers and Geotechnics, **61**, 132–143, 2014.
8. E. LIU, *Breakage and deformation mechanisms of crushable granular materials*, Computers and Geotechnics, **37**, 723–730, 2010.
9. Y. XIAO, H. LIU, J. ZHU, W. SHI, *Modeling and behaviours of rockfill materials in three-dimensional stress space*, Science China Technological Sciences, **55**, 2877–2892, 2012.

10. Y. LAI, M. LIAO, K. HU, *A constitutive model of frozen saline sandy soil based on energy dissipation theory*, International Journal of Plasticity, **78**, 84–113, 2016.
11. Y. SUN, B. INDRARATNA, J.P. CARTER, T. MARCHANT, S. NIMBALKAR, *Application of fractional calculus in modelling ballast deformation under cyclic loading*, Computers and Geotechnics, **82**, 16–30, 2017.
12. M. PASTOR, O.C. ZIENKIEWICZ, A.H.C. CHAN, *Generalized plasticity and the modelling of soil behaviour*, International Journal for Numerical and Analytical Methods in Geomechanics, **14**, 151–190, 1990.
13. A. GAJO, D. MUIR WOOD, *Severn-Trent sand: a kinematic-hardening constitutive model: the q - p formulation*, Géotechnique, **49**, 595–614, 1999.
14. Y. SUN, Y. XIAO, *Fractional order plasticity model for granular soils subjected to monotonic triaxial compression*, International Journal of Solids and Structures, **118–119**, 224–234, 2017.
15. X. LI, Y. DAFALIAS, *Dilatancy for cohesionless soils*, Géotechnique, **50**, 449–460, 2000.
16. V. BANDINI, M.R. COOP, *The influence of particle breakage on the location of the critical state line of sands*, Soils and Foundations, **51**, 591–600, 2011.
17. F. YU, *Particle breakage and the critical state of sands*, Géotechnique, **67**, 713–719, 2017.
18. A.R. RUSSELL, N. KHALILI, *A bounding surface plasticity model for sands exhibiting particle crushing*, Canadian Geotechnical Journal, **41**, 1179–1192, 2004.
19. Y.P. YAO, H. YAMAMOTO, N.D. WANG, *Constitutive model considering sand crushing*, Soils and Foundations, **48**, 603–608, 2008.
20. W. ZHOU, L. YANG, G. MA, X. CHANG, Y. CHENG, D. LI, *Macro–micro responses of crushable granular materials in simulated true triaxial tests*, Granular Matter, **17**, 497–509, 2015.
21. N. RODRIGUEZ, P. LADE, *True triaxial tests on cross-Anisotropic deposits of fine Nevada sand*, International Journal of Geomechanics, **13**, 779–793, 2013.
22. H.L. FANG, H. ZHENG, J. ZHENG, *Micromechanics-based multimechanism bounding surface model for sands*, International Journal of Plasticity, **90**, 242–266, 2017.
23. A. GAJO, D. MUIR WOOD, *A kinematic hardening constitutive model for sands: the multi-axial formulation*, International Journal for Numerical and Analytical Methods in Geomechanics, **23**, 925–965, 1999.
24. H.P. FEIGENBAUM, Y.F. DAFALIAS, *Directional distortional hardening at large plastic deformations*, International Journal of Solids and Structures, **51**, 3904–3918, 2014.
25. Y. XIAO, H. LIU, Y. CHEN, J. CHU, *Influence of intermediate principal stress on the strength and dilatancy behavior of rockfill material*, Journal of Geotechnical and Geoenvironmental Engineering, **140**, 04014064, 2014.
26. Y.P. YAO, Y.X. KONG, *Extended UH Model: three-dimensional unified hardening model for anisotropic clays*, Journal of Engineering Mechanics, **138**, 853–866, 2012.
27. Y. YAO, N. WANG, *Transformed stress method for generalizing soil constitutive models*, Journal of Engineering Mechanics, **140**, 614–629, 2014.
28. Y.P. YAO, W. HOU, A.N. ZHOU, *UH model: three-dimensional unified hardening model for overconsolidated clays*, Géotechnique, **59**, 451–469, 2009.

29. D. LU, C. MA, X. DU, L. JIN, Q. GONG, *Development of a new nonlinear unified strength theory for geomaterials based on the characteristic stress concept*, International Journal of Geomechanics, **17**, 04016058, 2016.
30. C. MA, D. LU, X. DU, A. ZHOU, *Developing a 3D elastoplastic constitutive model for soils: A new approach based on characteristic stress*, Computers and Geotechnics, **86**, 129–140, 2017.
31. N. KHALILI, M.A. HABTE, S. VALLIAPPAN, *A bounding surface plasticity model for cyclic loading of granular soils*, International Journal for Numerical Methods in Engineering, **63**, 1939–1960, 2005.
32. M. KAN, H. TAIEBAT, N. KHALILI, *Simplified mapping rule for bounding surface simulation of complex loading paths in granular materials*, International Journal of Geomechanics, **14**, 239–253, 2014.
33. J.P. CARTER, J.R. BOOKER, C.P. WROTH, *A critical state soil model for cyclic loading*, G.N. Pande, O.C. Zienkiewicz [eds.], *International Symposium on Soils Under Cyclic and Transient Loading*, pp. 219–252, John Wiley & Sons Ltd, Swansea, Wales, United Kingdom, 1982.
34. Y. SUN, Y. SHEN, *Constitutive model of granular soils using fractional order plastic flow rule*, International Journal of Geomechanics, **17**, 04017025, 2017.
35. D. LU, J. LIANG, X. DU, C. MA, Z. GAO, *Fractional elastoplastic constitutive model for soils based on a novel 3D fractional plastic flow rule*, Computers and Geotechnics, **105**, 277–290, 2019.
36. W. SUMELKA, M. NOWAK, *Non-normality and induced plastic anisotropy under fractional plastic flow rule: a numerical study*, International Journal for Numerical and Analytical Methods in Geomechanics, **40**, 651–675, 2016.
37. W. SUMELKA, *Fractional viscoplasticity*, Mechanics Research Communications, **56**, 31–36, 2014.
38. W. SUMELKA, *A note on non-associated Drucker-Prager plastic flow in terms of fractional calculus*, Journal of Theoretical and Applied Mechanics, **52**, 571–574, 2014.
39. Y. SUN, Y. GAO, Q. ZHU, *Fractional order plasticity modelling of state-dependent behaviour of granular soils without using plastic potential*, International Journal of Plasticity, **102**, 53–69, 2018.
40. Y. TIAN, Y.P. YAO, *Modelling the non-coaxiality of soils from the view of cross-anisotropy*, Computers and Geotechnics, **86**, 219–229, 2017.
41. I. PODLUBNY, *Fractional differential equations: an introduction to fractional derivatives, fractional differential equations, to methods of their solution and some of their applications*, Academic Press, San Diego, California, 1998.
42. K. BEEN, M.G. JEFFERIES, *A state parameter for sands*, Géotechnique, **35**, 99–112, 1985.
43. Y. ZHANG, H. SUN, H.H. STOWELL, M. ZAYERNOURI, S.E. HANSEN, *A review of applications of fractional calculus in Earth system dynamics*, Chaos, Solitons and Fractals, **102**, 29–46, 2017.
44. B.M. VINAGRE, I. PODLUBNY, A. HERNANDEZ, V. FELIU, *Some approximations of fractional order operators used in control theory and applications*, Fractional Calculus and Applied Analysis, **3**, 231–248, 2000.

-
45. K. ISHIHARA, *Liquefaction and flow failure during earthquakes*, Geotechnique, **43**, 351–451, 1993.
 46. R. WAN, P. GUO, *A simple constitutive model for granular soils: modified stress-dilatancy approach*, Computers and Geotechnics, **22**, 109–133, 1998.
 47. Z. WANG, Y. DAFALIAS, X. LI, F. MAKDISI, *State pressure index for modeling sand behavior*, Journal of Geotechnical and Geoenvironmental Engineering, **128**, 511–519, 2002.
 48. X. LI, Y. WANG, *Linear representation of steady-state line for sand*, Journal of Geotechnical and Geoenvironmental Engineering, **124**, 1215–1217, 1998.
 49. A. SCHOFIELD, P. WROTH, *Critical state soil mechanics*, McGraw-Hill London, New York, USA, 1968.
 50. B. HARDIN, J.F. RICHART, *Elastic wave velocities in granular soils*, Journal of Soil Mechanics and Foundations Division, ASCE, **89**, 33–66, 1963.
 51. V.E. TARASOV, *On chain rule for fractional derivatives*, Communications in Nonlinear Science and Numerical Simulation, **30**, 1–4, 2016.
 52. D.C. DRUCKER, W. PRAGER, H.J. GREENBERG, *Extended limit design theorems for continuous media*, Quarterly of Applied Mathematics, **9**, 381–389, 1952.
 53. R. VERDUGO, K. ISHIHARA, *The steady state of sandy soils*, Soils and Foundations, **36**, 81–91, 1996.
 54. H. MATSUOKA, T. NAKAI, *Stress-deformation and strength characteristics of soil under three different principal stresses*, Proceedings of the Japan Society of Civil Engineers, **232**, 59–70, 1974.
 55. Y. XIAO, H. LIU, Y. SUN, H. LIU, Y. CHEN, *Stress–dilatancy behaviors of coarse granular soils in three-dimensional stress space*, Engineering Geology, **195**, 104–110, 2015.

Received October 18, 2018; revised version January 23, 2019.

Published online February 27, 2019.
